CFD Validation for eVTOL Propeller Performance and Acoustics

Geng Qiao, G.Qiao.1@research.gla.ac.uk CFD Laboratory, School of Engineering, University of Glasgow, Scotland, UK
George N. Barakos, George.Barakos@glasgow.ac.uk, CFD Laboratory, School of Engineering, University of Glasgow, Scotland, UK

Abstract

Today, most innovative eVTOL designs, such as those with distributed propulsion systems, are equipped with multiple rotors and propellers. This introduces complex interactional aerodynamics and aeroacoustics that remain largely unexplored and not fully comprehended. This work starts from the discussion of the efforts made by the GARTEUR Action Group AG-26 to address the issue of noise generation and propagation in isolated and multirotor systems. The University of Glasgow, as a member of the action group, has focused on developing and validating numerical methods based on test data obtained by the experimental team at DLR's Acoustic Wind Tunnel Braunschweig (AWB). A comprehensive series of validation studies was conducted on the DLR 13x7 rotor in isolated hover, edge-wise flight, coplanar and tandem configurations with shifts in the two directions. The results substantiate the capability of the HMB3 tool to accurately resolve interactional aerodynamics, and the applied simulation strategy is sufficient to capture noise emissions at the experimental level. Additionally, the validation included conformal folding high lift propeller and cruise efficient wing designs from the X-57 aircraft, and the NASA Workshop for Integrated Propeller Prediction (WIPP), showcasing the capabilities and accuracy of the HMB3 tools, and the simulation strategy used, even when addressing cases involving installation effects. Employing the same approach, subsequent explorations included distributed propulsion systems. The incorporation of single and multiple propellers into the lifting surface has revealed that overwing configurations demonstrate lower propeller performance. However, the performance from the lifting surface experiences a marked enhancement, particularly at higher RPMs, resulting in an better propulsive efficiency.

1 Introduction

Research into aerodynamically generated noise attracts significant interest from industry, academia, and the government [1] [2]. One of the most promising markets in this regard is the growing Urban Air Mobility (UAM) sector, particularly concerning electric vertical take-off and landing (eVTOL) vehicles, due to their zero-emission capabilities and enhanced safety features. However, public acceptance of the noise emitted by such vehicles is crucial. The impetus for this study arises from the demand for increased efficiency, reduced noise, and enhanced safety in VTOL aircraft.

Novel vehicle concepts incorporate wing-tip-mounted propellers, distributed propulsion systems, and tandem rotors, introducing more intricate flow phenomena. Consequently, high-precision simulation results and comprehensive experimental databases are indispensable for quantifying and comprehending these complex interactions.

In an effort to bridge the knowledge gap in propeller and wing interactions, tests in the Lockheed Martin low-speed wind tunnel were conducted [3]. The test model of the Workshop for Integrated Propeller Prediction (WIPP) featured a semi-span wing measuring 67 inches, and a wing tip mounted C-130 propellers scaled at 10% of the actual size. Detailed measurements of all forces and moments were collected at various angles of attack and thrust settings. Validation for the WIPP case using the HMB3 CFD solver showing a good agreement, as presented in the work by Qiao and Barakos [4].

In a distributed propulsion system, it is possible to use smaller propellers compared to those used in a simple tip-mounted configuration [5]. Litherland and colleagues [6] conducted wind tunnel tests on a conformal high-lift propeller (HLP) designed for use with the X-57 "Maxwell" electric aircraft's distributed propulsion system. The X-57 utilises twelve fixed-pitch, conformal, high-lift propellers mounted into the wing leading edge to increase lift at low speeds. The conformal design enables the blades to fold into nacelle during cruise, reducing drag and performance losses. The experiments involved recording the performance of conformal high-lift propeller at various advance ratios and compared it with low and high order prediction mod-

Presented at 49th European Rotorcraft Forum, Germany, 5-7th September, 2023.

els [3] [7]. Although this work investigated the isolated configuration at axial forward conditions, performance variations and interactions from edgewise flight conditions and multiple propellers configurations should also be assessed.

Over the past decade, several studies demonstrated that hybrid-electric propulsion, when integrated efficiently into a propulsion system, can mitigate the impact of traffic-related pollution. However, such complex configurations also introduces intricate flow phenomena and interactions. In 2021, Vries et al. [8] conducted an experimental investigation of over-the-wing (OTW) propellers and their interactions with the boundary layer. Their experiment positioned the OTW propeller above the wing's hinge line. Measurements were conducted both with and without axial pressure gradients. Additionally, both time-averaged and unsteady interaction effects were quantified. The findings indicated that the propeller positioned over the wing generated an adverse pressure gradient on the wing surface, linearly proportional to the thrust. Consequently, increasing the blade-tip clearance resulted in a decrease in thrust. The authors attributed this pressure gradient, at least in part, to slipstream contraction, which led to deceleration of the flow near the wing's surface. Moreover, the presence of the propeller blades induced fluctuations in surface pressure and caused an increase in the time-averaged pressure due to flow deceleration. The study also examined various propeller locations, revealing that increasing the tip clearance did not effectively mitigate flow separation. Conversely, positioning the propeller half a radius upstream of the hinge line generated a Coanda effect, causing the flow to attach to the flap surface due to suction. This effect further contributed to an increment in lift for the entire configuration.

The benefits and drawbacks of transitioning from conventional tractor to over-the-wing configurations were not fully assessed in earlier studies. Consequently, future designs may lack certainty regarding which configurations to adopt.

This study builds upon the findings of the WIPP [3], conformal HLP experiments [6], and the investigations of the GARTEUR Action Group 26 (AG26) project [1]. Its objective is to optimise propulsion systems equipped with single and multiple propellers/rotors, installed in various configurations, using high-fidelity methods. Flow interaction visualisations and loading analyses are conducted to illustrate the interactions that arising from different designs, as well as the corresponding performance variations. Furthermore, this research addresses the need for a comprehensive assessment of the trade-offs and advantages associated with both conventional and over-the-wing configurations. The study goes beyond isolated investigations and strives to provide a systematic comparison, facilitating an informed decision-making process for future aircraft designs. Ultimately, this research endeavors to contribute to the advancement of environmentally friendly and efficient propulsion solutions for the aviation industry.

2 Methodology

The in-house Helicopter Multi-Block (HMB3) code is employed in this study. The solver can accurately predict the aerodynamic performance and acoustics of propagation, as shown in previous studies [9, 10]. HMB3 has been widely used in the investigation of rotorcraft flows [11, 12, 13, 14], helicopter rotor aeroelasticity [15], propeller aeroacoustics [16], flight mechanics [17] and missile trajectory prediction [18]. Moreover, a good agreement when compared to experimental results in aerodynamics, acoustics and aeroelasticity of propellers, which can be seen in previous studies [19, 20, 21, 22]. Most recently, its ability to capture the interactions of multi-rotor flows and ducted propeller flows was documented [23, 24, 25, 26, 27]. HMB3 solves the Unsteady Reynolds Averaged Navier-Stokes(URANS) equation in integral form using the Arbitrary Lagrangian-Eulerian formulation for time-dependent domains, including moving boundary layers. HMB3 uses a cell-centred finite volume approach to discrete Navier-Stokes equations on multi-block, structured grids.

$$\frac{d}{dt}\left(\mathbf{W}_{i,j,k}V_{i,j,k}\right) = -\mathbf{R}_{i,j,k}\left(\mathbf{W}_{i,j,k}\right), \tag{1}$$

In Equation (1), i,j,k represent the cell index, $\mathbf{W}$ and $\mathbf{R}$ are the vector of conservative flow variables and residual respectively, and $V_{i,j,k}$ is the volume of the cell i,j,k. The convective fluxes are evaluated using the Osher approximate Riemann solver, while the viscous terms are discretised using a second-order central difference scheme. The third-order MUSCL (Monotone Upstream-centered Schemes for Conservation Laws) approach is applied to provide high-order accuracy in space. In the present work, simulations are conducted using the $k-\omega$ shear stress transport (SST) turbulence model [28] turbulence model as this has been well validated in the current and previous studies for the interactional aerodynamics [4, 29].

For the validation of the isolated DLR 13x7 rotor at hover and axial forward flight simulations, the azimuthal symmetry of the configuration can be exploited, whereby only a fraction of the grid needs to be generated. The Rotating Reference Frame (RRF) method is implemented in HMB3 [30] for simulations with rotational periodicity. The governing flow equations are reformulated and solved in a non-inertial rotating reference frame, thus transforming the unsteady problem into steady calculations. For the unsteady simulations, the entire grid is required. However, this can be obtained by copying and rotating the grids of the steady simulations using HMB3 tool. Additionally, unsteady calculations have applied the implicit dual-time stepping approach.

Present work calculates the near-field acoustics information from the resolved pressure fields, which are computed with the high-fidelity simulation code HMB3. Then, the sound pressure signal is obtained by subtracting the time-averaged pressure field solution. To accurately predict the acoustics, refined spatial/temporal resolution is required by applying a high-order scheme; hence a 3rd-order MUSCL scheme is applied for the current acoustic study. In addition, CFD grids are applied and guaranteed to have at least 20 cells for wavelength targeting (four times the Blade Passing Frequency (BPF)). Moreover, a well-steady convergence or a proper time step is confirmed. This approach has also been applied to previous work by Chirico *et al.* [31] [32], Zhang and Barakos [25]. More acoustics predictions and noise reduction work was also conducted by Smith *et al.*in 2020 [33].

Furthermore, to assess the mutual influence between propellers and the lifting surface, it is evident that both components of each configuration cannot be independently evaluated. Thus, an integration of relevant forces (Thrust T, drag D) should be employed to comprehensively compare the overall performance of different configurations.

In the following equation Equation (2), the overall installed thrust (T_{install}) is calculated by subtracting the drag ($D_{\text{lifting surface}}$) created by the lifting surface from the total thrust ($T_{\text{propellers}}$) generated by the propellers.

$$T_{install} = T_{propellers} - D_{lifting\,surface} \tag{2}$$

Subsequently, the overall propulsive efficiency can be simplified, This can be seen in Equation (3). Here, V_∞ represents the freestream velocity, and P_{shaft} denotes the power required by the power shaft.

$$Overall\ propulsive\ efficiency\ (\eta) = \frac{T_{install} \times V_\infty}{P_{shaft}} \tag{3}$$

Finally, this study will apply the aforementioned equations to evaluate the overall performance of equivalent tractor and overwing distributed propulsion systems, with ensuring that the lifting surface is trimmed to produce the same lift.

3 CFD Validation

This section presents the CFD grids and computation setups utilised for isolated and full rotor simulations, along with their background for axial flight and edge-wise cruise simulations. For axial flight cases, the computation domain and microphone positions depicted in Figure 1 are employed. Furthermore, Figure 2 illustrates the full rotor geometry and its grid topology used for the cruise simulations with isolated and multi-rotor systems. To understand the sensitivities of the performance and acoustics results to their grid, a mesh convergence study was performed on the full rotor axial flight simulations, as shown in Table 1.

Given the aerodynamic and aeroacoustic tests conducted by Litherland et al. [6] at the NASA Langley Research Centre with the Low-Speed Aeroacoustic Wind Tunnel, the current work involved numerical studies for the conformal folding High Lift Propeller (HLP). The HLP has five blades with a radius of 0.288 m and a pitch angle of 24.1 degrees at 75% of the blade radius. Advance ratios from 0.65 to 1.17 were tested with varying RPM from 4200 to 4800 and flight velocities from $30m/s$ to $54m/s$. The geometry details and schematic diagram of the propeller were described by Qiao et al. [29]. The HMB3 CFD method was used to predict performance, as shown in Figure 3. Aerodynamic coefficients were compared against the experiments with various advance ratios, and a good agreement can be observed between HMB3 predictions and the experimental results. [6]

For the DLR experiments, the flow from single-blade simulations is visualised, and aerodynamic loads [34] are cross-plotted with experimental data [35] in Figures 4. Additionally, the velocity field is averaged through one revolution, similarly to fixed PIV windows in wind tunnels [36]. Extracted slices from -0.1R and -0.6R in Figure 5 show similar trends to the PIV data from CIRA/DLR joint experimental campaign. [36] (PIV data acquired from CIRA/DLR joint experimental campaign on DLR rotor rig and performed at CIRA laboratories using CIRA PIV measurement system.) The agreement between the simulation and experimental data confirming the accuracy and reliability of the HMB3 CFD method in predicting the aerodynamic performance of the DLR 13x7 rotor.

Looking at acoustic predictions, the comparison of the Overall Sound Pressure Level (OSPL) and frequency spectra with wind tunnel tests at various microphone locations are shown in Figure 6. It is evident that the current simulation strategy agrees well with the measured data from microphones obtained by experiments conducted by DLR [37] [38] [39]. Notably, the noise from the wake region is particularly well captured by the simulations.

The mesh convergence study further reveals that the cell size used are sufficient to capture the noise, except for the area directly under the rotor. Refining the grid in three directions, from Grid 3, led to better noise predictions at the rotor tip region, indicating that small cell spacing is required for the high-speed and wake regions. The grid refinement significantly improved the predicted results, bringing them closer to the experimental data.

Overall, the grids used for axial and cruise simulations, demonstrated that the applied method and grids in this work are of sufficient accuracy. The agreement between simulation and experimental data confirmed the reliability of the numerical approach in accurately predicting the acoustics of high RPM rotors.

In addition to the axial flight simulations, this work also includes the validation of the 13x7 DLR rotor [37] at several edge-wise cruise flight conditions, along with a time step convergence study, as shown in Figures 7. The flow visualisations top and side views show that the isolated rotor at edge-wise flight is well resolved at an advance ratio of 0.073, particularly in the wake region.

Furthermore, noise directivity is extracted from the HMB3 results and compared with experimental and predicted results from DLR. The findings from the current work indicate that a time step of 1 degree per step yields similar Sound Pressure Level (SPL) as the 2-degree per step case. However, the 1-degree simulation predicts slightly higher SPL at rpm 12,000. Nevertheless, all applied time step sizes in this work are sufficient to capture the noise directivity at different flight speeds and conditions.

Table 1: Summary of the grid sizes used for GARTEUR AG26 DLR 13x7 rotor axial flight validation cases.

Grid Component	Grid 1	Grid 2	Grid 3
Rotor	4.7	6.0	7.0
Background	3.0	6.2	12.00
Total	7.7	12.2	19.0

Table 2: Summary of the grid sizes used for GARTEUR AG26 DLR 13x7 rotor validation tandem configurations.

Grid Component	Grid Cells
Rotor 1	4.7
Rotor 2	4.7
Local Refinement 1	0.8
Local Refinement 2	0.8
Near-field	6.6
Far-field	0.7
Total	18.3

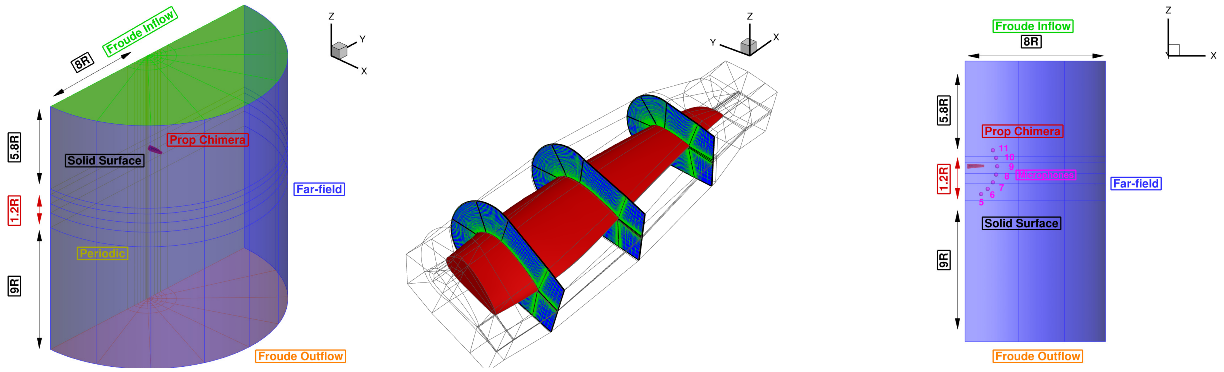

(a) Background Mesh topology. (b) Single blade mesh topology. (c) Microphones positions.

Figure 1: Grids and microphones used for single blade steady simulations.

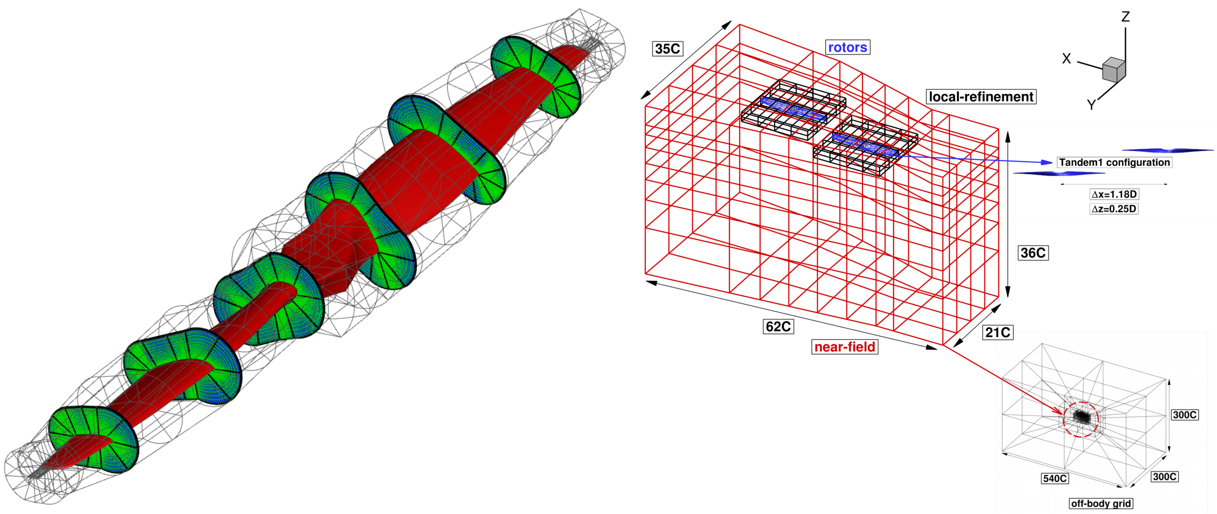

(a) Full rotor mesh topology. (b) Tandem1 configuration.

Figure 2: Grid topology used for HMB3 simulations of the GARTEUR AG26 multi-rotor cases.

Nowadays, most novel eVTOL designs, such as those with distributed propulsion systems, are equipped with multiple rotors/propellers, which introduces interactional aerodynamics and aeroacoustics. Consequently, validation work has been undertaken to include multi-rotor systems. The initial grids and time step refinement study conducted in this work have proved beneficial for further multi-rotor studies.

Flow interactions and noise emissions of tandem rotors, both with and without vertical offsets, are shown in Figure 8. From the obtained results, it can be observed that the wake from the upstream rotor is affecting the downstream rotor, resulting in more complex interactions. A vertical offset for the downstream rotor leads to microphones 2 and 3 become quieter as the downstream rotor is not directly affected by the wake from the upstream rotor, hence less aerodynamic interactions.

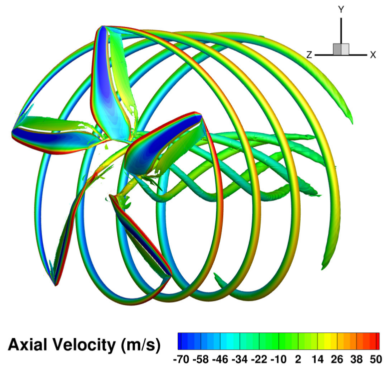

(a) Wake visualisation at the condition with advance ratio equals 0.84.

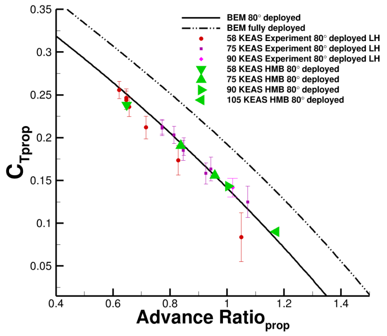

(b) Thrust coefficient variations with propeller advance ratios for the HLP.

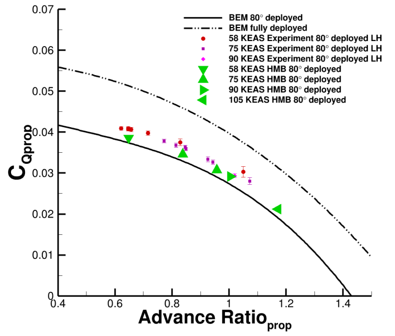

(c) Torque coefficient variations with propeller advance ratios for the HLP.

Figure 3: Aerodynamic coefficient variations with propeller advance ratios for the HLP. [6]

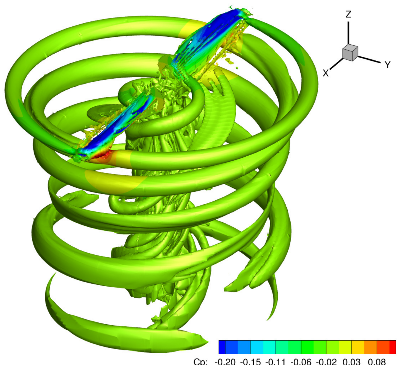

(a) Wake visulisation at RPM 12,000.

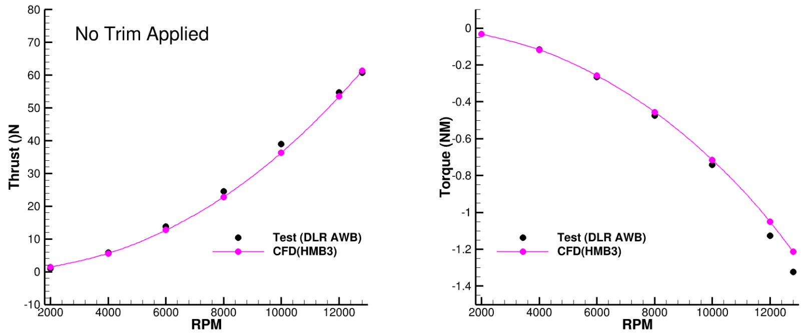

(b) Thurst and torque comparison.

Figure 4: GARTEUR AG26 13x7 rotor validation studies for RPM from 2,000 to 12,800 using UoG high-fidelity tool HMB3 and compared with DLR's Acoustic wind tunnel Braunschweig (AWB) data [35].

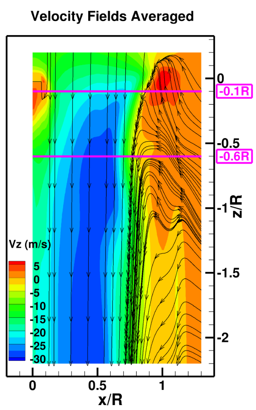

(a) Velocity filed.

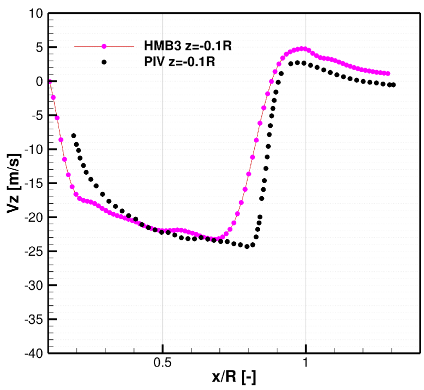

(b) Extracted slice from -0.1R.

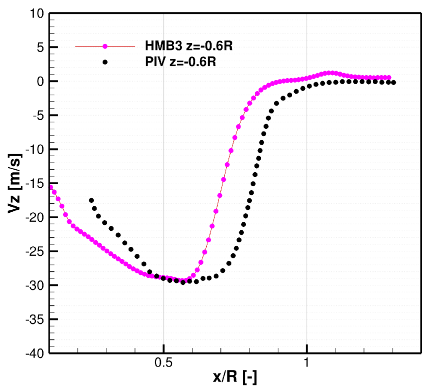

(c) Extracted slice from -0.6R.

Figure 5: (a) Averaged velocity field results from HMB3 with fixed PIV window. (b)(c) Extracted velocity profile from the wake region at distance -0.1R and -0.6R, and compared with PIV data acquired from CIRA/DLR joint experimental campaign on DLR rotor rig and performed at CIRA laboratories using CIRA PIV measurement system [36].

The aerodynamic performance of the upstream rotor shows minimal changes, compared to a reduced performance of the downstream rotor, for coplanar configuration, as shown in Figure 9.

The investigation of multi-rotor configurations is essential for understanding the aerodynamic and aeroacoustic behaviors of advanced eVTOL designs, especially those with distributed propulsion systems.

4 Distributed Propulsion

This section presents further investigations into different distributed propulsion systems with one and multiple propellers installed. The setups for these propulsion systems are given in Figure 10. The installed High Lift Propeller (HLP) has been previously validated in the `section 3` [29], and the lifting surface is extracted from the NASA X-57 cruise-efficient wing, which has also undergone validation in previous WIPP studies

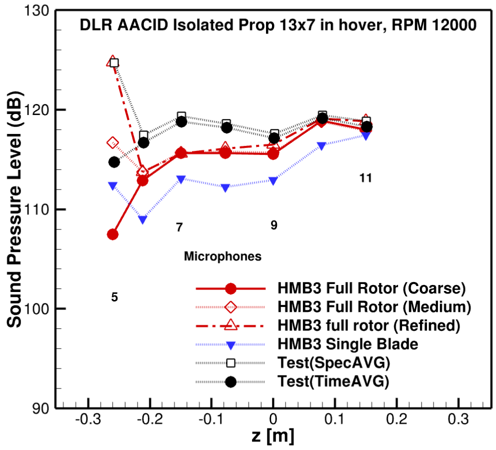

(a) OSPL comparison.

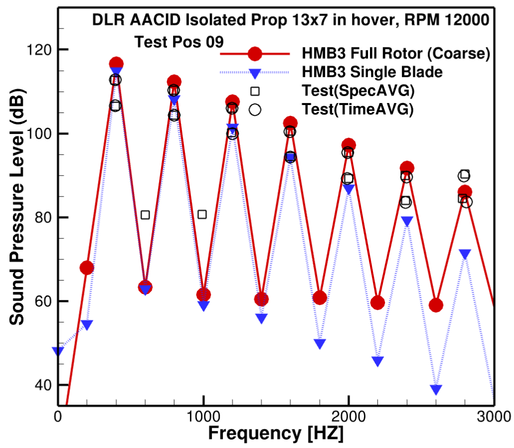

(b) Microphone 9.

Figure 6: (a) OSPL results comparisons using single blade, full rotor and multiple grid resolutions. (b) Frequency spectra at axial flight case with RPM 12,000 obtained using HMB3 tool and compared with experiments from DLR's Acoustic wind tunnel Braunschweig (AWB) [35].

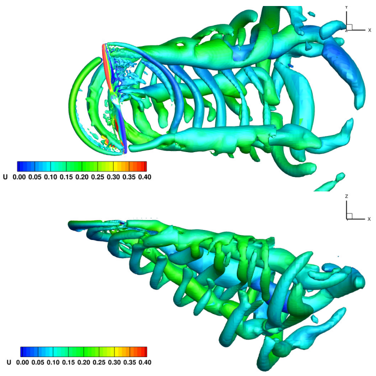

(a) Wake visualisation at the condition with advance ratio equals 0.073 and RPM equals 8000.

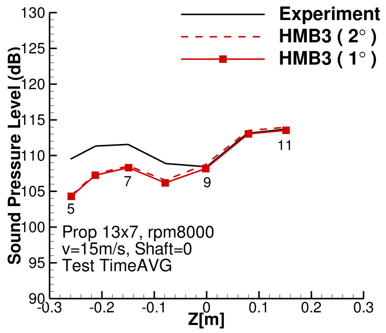

(b) OSPL at the condition with advance ratio equals 0.073 and RPM equals 8000.

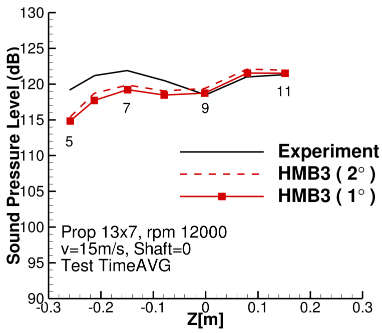

(c) OSPL at the condition with advance ratio equals 0.109 and RPM equals 12000.

Figure 7: (a) Wake Visulisation at RPM 8,000. (b)(c) Time step refinement study of the 13x7 DLR rotor edgewise forward flying at 15m/s with RPM from 8,000 to 12,000 using HMB3 tool, and compared with DLR's Acoustic wind tunnel Braunschweig (AWB) data [35].

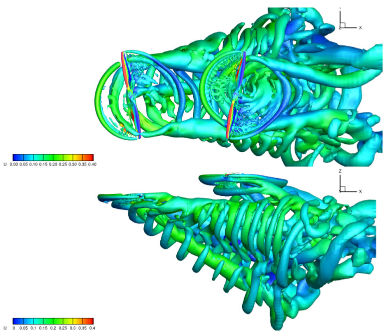

(a) Wake visualisation at the tandem vertical off-set configuration.

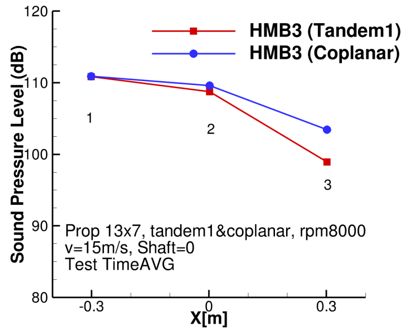

(b) OSPL comparison.

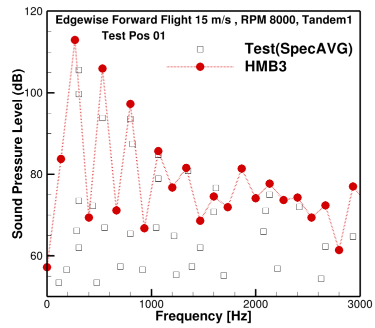

(c) Microphone 1.

Figure 8: (a) Wake visulisation. (b) OSPL comparisions at three different microphones from coplanar and tandem with vertical off-set cases. (c)Acoustics spectra analysis of 13x7 DLR rotor edgewise forward flying at 15m/s with RPM 8,000, and compared with DLR's Acoustic wind tunnel Braunschweig (AWB) data [35].

[4]. With confidence in using the same CFD tools and grid resolution from the previous validations, the following work will focus on studying the aerodynamic performance and aeroacoustic characteristics of distributed tractor and overwing propulsion systems with optimised propeller locations, were studied.

Flow visualisation from the distributed propulsion systems with two propellers installed in tractor, over-

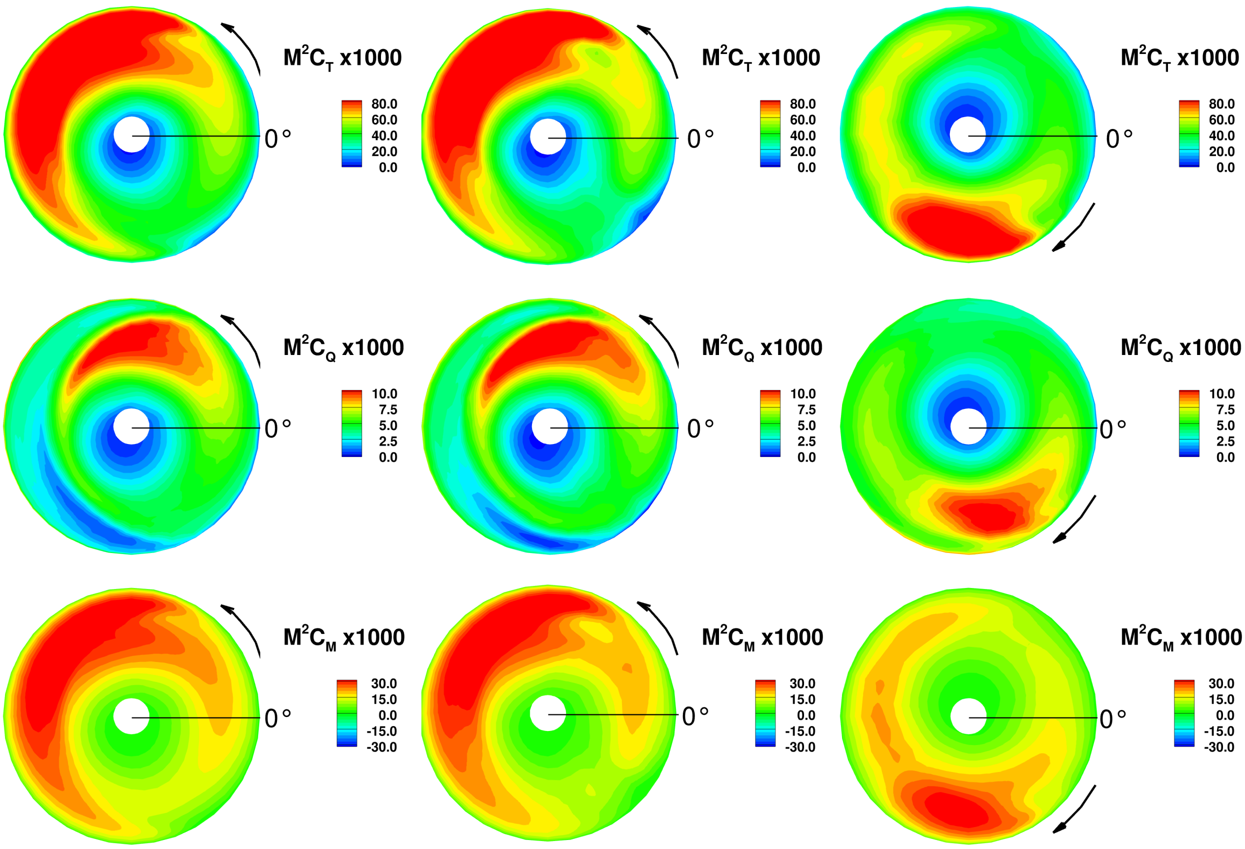

(a) Isolated rotor. (b) Coplanar upstream rotor. (c) Coplanar downstream rotor.

Figure 9: Pi plots of DLR 13x7 rotor contoured with thurst, torque and pithch up moment coefficients at the edge-wise flight with advance ratio = 0.073, and the RPM = $8,000$.

wing configurations and three propellers installed overwing, can be seen in Figures 12, 13 at axial forward flight condition with an advance ratio of 0.42. Strong aerodynamic interference is noticed in the tractor configuration compared to the overwing configuration. Performance data from single propeller installed propulsion systems at high-performance forward flight conditions is presented in Table 3. Both configurations have been trimmed to generate a similar amount of lift, and the lift-to-drag ratio has increased by 3 times with the over-wing propeller installed propulsion system. Additionally, the propeller performance from the overwing case has dropped slightly, but the overall propulsive efficiency has improved significantly.

Further investigations assess the performance of the tractor and overwing propulsion systems with two propellers installed. Aerodynamic loads from the overall propulsion system and their individual components are presented in Table 4. The results show that the benefit in lift-to-drag ratio can still be seen from the overwing configuration. Although the propeller performance drops in the overwing configuration, the overall propulsive efficiency is still much higher than the tractor propulsion system.

Furthermore, by distributing the thrust and lift from single to two propellers, the vorticity magnitude shown in Figure 11 demonstrates a significant reduction in vorticity. This results in a lower tip speed for the distributed propulsion system, which is important as the propeller/rotor noise is highly dependent on the tip speed.

With the optimal overwing distributed propulsion system in place, further investigation incorporates a third propeller and compares its performance with a two-propeller overwing configuration, as presented in Figure 14(c). The figure illustrates that with the addition of another propeller and operating at a lower RPM, both configurations require a similar amount of power. However, when compared to the two-propeller case, the three-propeller case generates additional thrust, resulting in an increased Lift-to-Drag ratio (L/D) for the lifting surface. Furthermore, both propeller and overall propulsive efficiency experience significant improvements, indicating that a distributed propulsion system can indeed yield enhanced performance.

5 Conclusions

This work presented the aerodynamic and aeroacoustic validation of isolated and multi-rotor configurations at various conditions based on the GARTEUR AG26 [37] [38] [39], WIPP [3], and X57 projects [6]. The validation work is first summarised. Validations for the DLR 13x7 rotor and X57 High Lift Propeller (HLP) demonstrated that the HMB3 tool accurately predicted the aerodynamic performance and wake profiles across a wide range of RPM conditions, using both steady and unsteady simulation strategies. Further mesh refinement and time step refinement studies for the DLR 13x7 rotor in axial and edge-wise cruise flight condi-

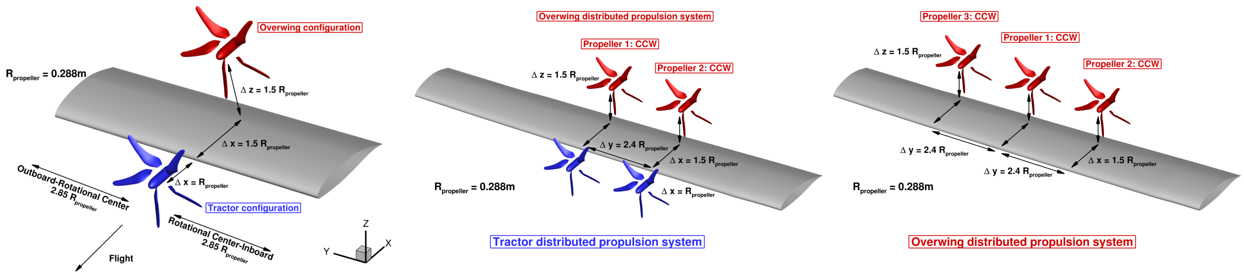

(a) Single propeller installed propulsion system.

(b) Two propellers installed propulsion systems.

(c) Three propellers installed overwing distributed propulsion system.

Figure 10: Schematic illustration of investigated distributed propulsion systems with single and multiple propellers installed.

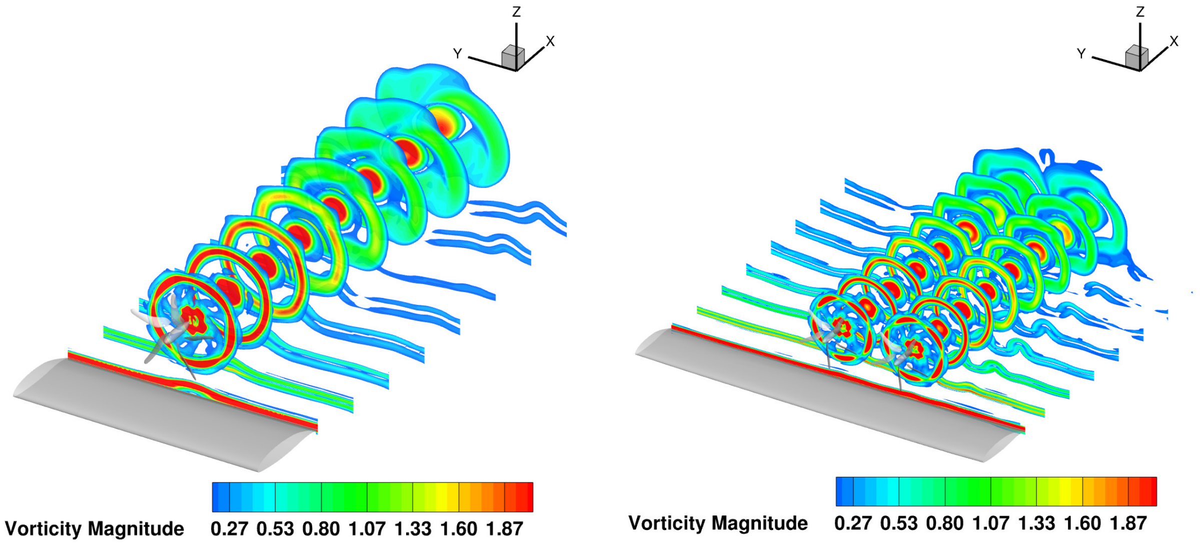

(a) Visulisation of vorticity magnitude of single installed over-wing configuration at advance ratio 0.19.

(b) Visulisation of vorticity magnitude of distributed over-wing configuration at advance ratio 0.23.

Figure 11: Visulisation of vorticity magnitude of single installed and distributed over-wing configurations at equivalent thrust condition.

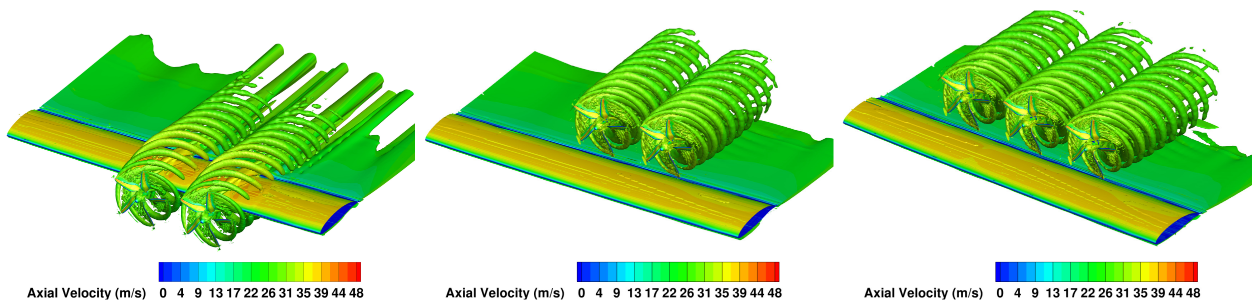

(a) Conventional tractor configuration.

(b) Overwing configuration.

(c) Overwing distributed propulsion system.

Figure 12: Flow visulisations of distributed tractor and over-wing configurations at advance ratio 0.42 using iso-surface of Q-criteria with value 0.01 contoured using axial velocity.

tions confirmed that the applied grid resolution and time step size are sufficient for accurately predicting noise emissions.

In addition, multi-rotor systems such as coplanar and tandem configurations with vertical offset were studied. The plots of the rotor performance from isolated and coplanar rotors indicated that the upstream rotor performance is similar to the isolated configuration, while the downstream rotor performance is reduced for coplanar configurations. The Sound Pressure Level (SPL) spectra at three microphones located from upstream to downstream showed similar trends compared to wind tunnel measured results. Comparing the Overall Sound Pressure Level (OSPL) from the investigated microphones, the tandem rotors with vertical offset were much quieter than the coplanar configurations at microphones 2 and 3, apparently due to the fewer aerodynamic interactions occurring.

With confidence in the CFD methods and grids

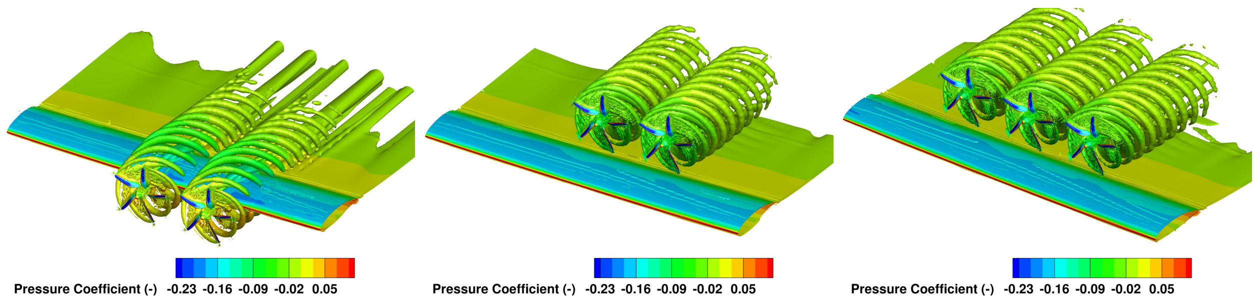

(a) Conventional tractor configuration. (b) Overwing configuration. (c) Overwing distributed propulsion system.

Figure 13: Flow visulisations of distributed tractor and over-wing configurations at advance ratio 0.42 using iso-surface of Q-criteria with value 0.01 contoured using pressure coefficient.

Table 3: Performance comparison of the wing at different single propeller installed propulsion configuration.

Performance (RPM=4800)	Tractor	Overwing	Benefit of Overwing
Lift (N)	582	590	+1.3%
L/D (-)	15.2	60.0	+294%
Thurst (N)	257	238	-7.4%
Power (kW)	12.6	12.5	-0.8%
Propeller Froude efficiency (-)	0.56	0.52	-6.4%
Overall propulsive efficiency (-)	0.476	0.502	+5.5%

Table 4: Performance comparison of the wing at different tandem propellers installed distributed propulsion configuration.

Performance (RPM=3900)	Tractor	Overwing	Benefit of Overwing
Lift (N)	1140	1149	+0.7%
L/D (-)	15.74	30.20	+92%
Thurst (N)	308	273	-11.3%
Power (kW)	13.3	12.8	-3.8%
Propeller Froude efficiency (-)	0.64	0.59	-7.8%
Overall propulsive efficiency (-)	0.487	0.505	+3.8%

used in the validation studies, the same simulation strategy was applied the study distributed propulsion systems.

The summary of the investigation into distributed propulsion systems of various configurations follows. The study of a single HLP installed in tractor and overwing configurations shows that at the same RPM, the propeller of the tractor configuration generates higher thrust but requires more power than the overwing configuration, resulting in a higher propeller Froude efficiency in the tractor configuration. For the lifting surface component, the Lift-to-Drag ratio (L/D) increases when transitioning from the tractor to overwing configuration while generating the same lift. The overall propulsive efficiency applied to assess the integrated performance of the investigated configurations shows that the single propeller installed in the overwing configuration, has better overall efficiency.

Additional studies investigated two propellers installed in tractor and overwing configurations. Both propellers operated at lower RPM to produce the same level of thrust as the single propeller. In the case of the two propellers, the performance trends are similar to the single propeller-installed configuration. However, the Lift-to-Drag ratio (L/D) is reduced in the overwing configuration compared to the single propeller-installed case, hence reducing the RPM has also reduced the L/D of the lifting surface. This reduction indicates that the propellers in the overwing configuration create a more favorable flow environment for the lifting surface when compared with the tractor configuration, especially when operating at higher RPM. Finally, the overall efficiency of the entire configuration was better than the tractor configuration.

This enhancement in performance highlights the potential benefits of incorporating multiple propellers within the overwing configuration. The additional propeller contributes to increased thrust generation which requires a similar amount of power, thereby enhancing the propeller efficiency of the propulsion system. Moreover, the interaction between the propellers and the lifting surface becomes more favorable, resulting in improved lift-to-drag ratios (L/D) for the lifting surface itself.

In summary, the present study, employing high-fidelity methods, highlights the performance of both tractor and overwing configurations, considering single and multiple propellers installed in propulsion systems. This research has investigated the advan-

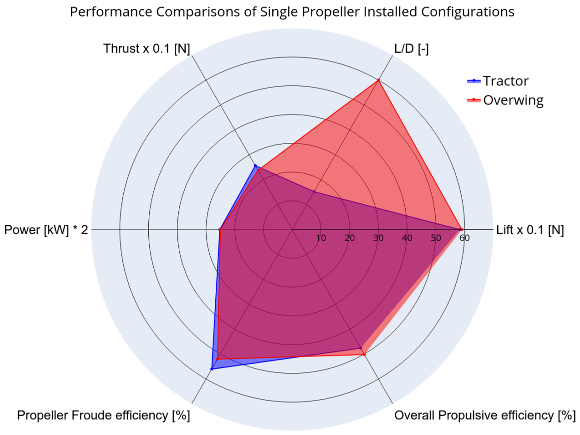

(a) Performance of single propeller installed propulsion systems at $RPM = 4800$.

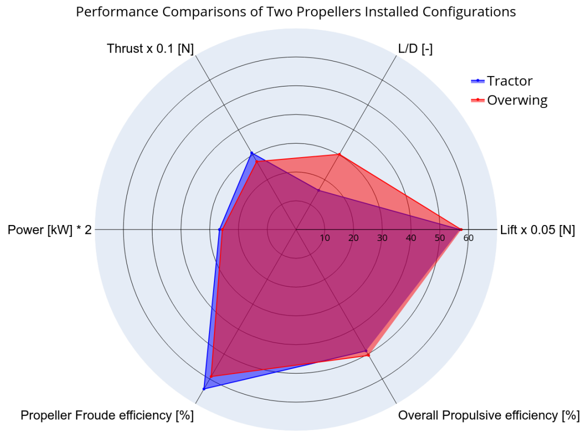

(a) Performance of two propellers installed propulsion systems at $RPM = 3900$.

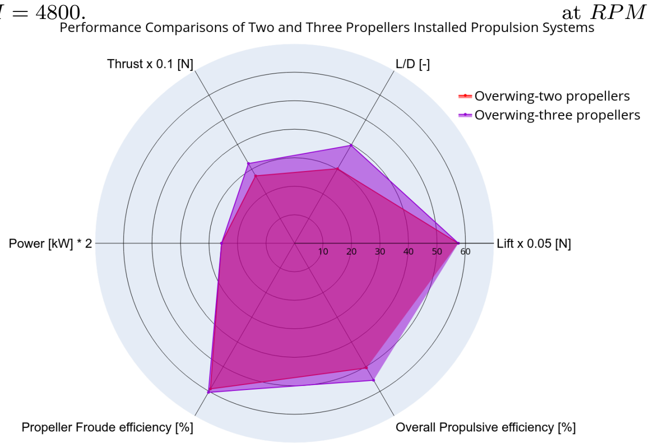

(a) Performance of two and three propellers installed propulsion systems at $RPM = 3900$ and $RPM = 3700$.

Figure 14: Comparisons of tractor and overwing configurations with single and multiple propellers installed propulsion systems.

tages and trade-offs inherent in various distributed propulsion configurations, offering valuable insights into optimising the aerodynamic performance of distributed propulsion systems at high-performance conditions. The investigation into the optimum overwing distributed propulsion system, with the addition of an extra propeller, demonstrates clear performance improvements.

Acknowledgments

The support of the Bill Nicol Engineering Scholarship from the University of Glasgow, and the financial support from the school of engineering are gratefully acknowledged. Some results obtained using the EPSRC-funded ARCHIE-WeSt High-Performance Computer (www.archie-west.ac.uk) is acknowledged. The geometry, experimental, and numerical results of the 13x7 rotor provided by Dr. Jianping Yin, Karl-Stéphane Rossignol, Schwarz Thorsten, and Lukas Rottmann of the German Aerospace Center (DLR), along with the PIV data from Fabrizio De Gregorio and Giuseppe Ceglia of the Italian Aerospace Research Centre (CIRA), as well as the GARTEUR AG26 partners are also acknowledged.

Bibliography

[1] Yin, J., Barakos, G., Qiao, G., De Gregorio, F., Petrosino, F., Rossignol, K.-S., Schwarz, T., Cotte, B.and Brouwer, H., Clero, F. Mortain, F., Vigevano, A., Schmahl, M., Kaltenbach, H.-K., Pagliaroli, T. Ragni, D., Rottmann, L., Ceglia, G., Reboul, G., Muth, M., Kessler, M., Visingardi, A., Barbarino, M., Petrosino, F., Zanotti, A., Oberti, N., Galimberti, L., Bernardini, G., Poggi, C., Abergo, L., Caccia, F., Guardone, A., Testa, C., and Zaghi, S., "Noise Radiation and Propagation for Multirotor System Configurations. In: Terms of Reference for the GARTEUR Action Group HC/AG-26," December 2021.

[2] Gutin, L., "On the Sound Field of a Rotating Propeller," *Physical magazine of the Soviet Union-NACA Technical Memorandum No.1195*, Vol. 9, No. 1, 1948.

[3] Hooker, J. R., Wick, A., Ginn, S. R., Walker, J., and Schiltgen, B. T., "Overview of Low Speed Wind Tunnel Testing Conducted on a Wingtip Mounted Propeller for the Workshop for Integrated Propeller Prediction," *AIAA AVIATION 2020 FORUM*, 2020, p. 2673.

[4] Qiao, G. and Barakos, G. N., "Verification and Optimisation of Distributed Propulsion Using High-Fidelity CFD Method," *American Helicopter Society 79th Annual Forum & Technology Display, May 16-18, 2023, West Palm Beach, Florida, USA*, 2023.

[5] Litherland, B. L., Patterson, M. D., Derlaga, J. M., and Borer, N. K., "A method for designing conforming folding propellers," *17th AIAA Aviation Technology, Integration, and Operations Conference*, 2017, p. 3781.

[6] Litherland, B. L., Borer, N. K., and Zawodny, N. S., "X-57 Maxwell High-Lift Propeller Testing and Model Development," *AIAA AVIATION 2021 FORUM, Virtual*, 2-6 August 2021, p. 3193.

[7] Litherland, B. L. and Derlaga, J. M., "A Performance Analysis of Folding Conformal Propeller Blade Designs," *AIAA Aviation 2019 Forum, Dallas, Texas, 17-21 June 2019*, 2019, p. 3676, 10.2514/6.2019-3676.

[8] de Vries, R., van Arnhem, N., Avallone, F., Ragni, D., Vos, R., Eitelberg, G., and Veldhuis, L. L., "Experimental Investigation of Over-the-Wing Propeller–Boundary-Layer Interaction," *AIAA Journal*, Vol. 59, No. 6, 2021, pp. 2169–2182.

[9] Steijl, R., Barakos, G., and Badcock, K., "A framework for CFD analysis of helicopter rotors in hover and forward flight," *International journal for numerical methods in fluids*, Vol. 51, No. 8, 2006, pp. 819–847.

[10] Biava, M., Woodgate, M., and Barakos, G. N., "Fully implicit discrete-adjoint methods for rotorcraft applications," *AIAA Journal*, Vol. 54, No. 2, 2016, pp. 735–749.

[11] Antoniadis, A., Drikakis, D., Zhong, B., Barakos, G., Steijl, R., Biava, M., Vigevano, L., Brocklehurst, A., Boelens, O., Dietz, M., et al., "Assessment of CFD methods against experimental flow measurements for helicopter flows," *Aerospace Science and Technology*, Vol. 19, No. 1, 2012, pp. 86–100.

[12] Steijl, R. and Barakos, G., "CFD analysis of complete helicopter configurations–lessons learnt from the GOAHEAD project," *Aerospace Science and Technology*, Vol. 19, No. 1, 2012, pp. 58–71.

[13] Han, D., Pastrikakis, V., and Barakos, G. N., "Helicopter flight performance improvement by dynamic blade twist," *Aerospace Science and Technology*, Vol. 58, 2016, pp. 445–452.

[14] Garcia, A. J. and Barakos, G. N., "Numerical simulations on the ERICA tiltrotor," *Aerospace Science and Technology*, Vol. 64, 2017, pp. 171–191.

[15] Dehaeze, F. and Barakos, G., "Mesh deformation method for rotor flows," *Journal of Aircraft*, Vol. 49, No. 1, 2012, pp. 82–92, DOI: 10.2514/1.C031251.

[16] Chirico, G., Barakos, G., and Bown, N., "Numerical aeroacoustic analysis of propeller designs," *The Aeronautical Journal*, Vol. 122, No. 1248, 2018, pp. 283–315, DOI: 10.1017/aer.2017.123.

[17] Crozon, C., Steijl, R., and Barakos, G., "Coupled flight dynamics and CFD - demonstration for helicopters in shipborne environment," *The Aeronautical Journal*, Vol. 122, No. 1247, 2018, pp. 42–82, DOI: 10.1017/aer.2017.112.

[18] Babu, S., Loupy, G., Dehaeze, F., Barakos, G., and Taylor, N., "Aeroelastic simulations of stores in weapon bays using Detached-Eddy Simulation," *Journal of Fluids and Structures*, Vol. 66, October 2016, pp. 207–228, DOI: 10.1016/j.jfluidstructs.2016.07.014.

[19] Barakos, G. and Johnson, C., "Acoustic comparison of propellers," *International Journal of Aeroacoustics*, Vol. 15, No. 6-7, 2016, pp. 575–594, DOI: 10.1177/1475472X16659214.

[20] Higgins, R., Jimenez-Garcia, A., Barakos, G., and Bown, N., "High-Fidelity Computational Fluid Dynamics Methods for the Simulation of Propeller Stall Flutter," *AIAA Journal*, Vol. 57, No. 12, 2019, DOI: 10.2514/1.J058463.

[21] Higgins, R., Barakos, G., and Jinks, E., "Estimation of Three-Dimensional Aerodynamic Damping using CFD," *The Aeronautical Journal*, Vol. 124, No. 1271, 2020, DOI: 10.1017/aer.2019.135.

[22] Higgins, R., Zarev, A., Barakos, G., and Green, R., "Numerical Investigation of a Two-Bladed Propeller Inflow at Yaw," *Journal of Aircraft*, Vol. 57, No. 2, 2020, DOI: 10.2514/1.C035647.

[23] Higgins, R., Barakos, G., Shahpar, S., and Tristanto, I., "An Aeroacoustic Investigation of a Tiltwing eVTOL Concept Aircraft," *AIAA Aviation 2020 Forum*, AIAA, 2020, DOI: 10.2514/6.2020-2684.

[24] Zhang, T. and Barakos, G. N., "High-fidelity CFD validation and assessment of ducted propellers for aircraft propulsion," *Journal of the American Helicopter Society*, Vol. 66, No. 1, 2021, pp. 1–28.

[25] Zhang, T. and Barakos, G. N., "High-fidelity numerical analysis and optimisation of ducted propeller aerodynamics and acoustics," *Aerospace Science and Technology*, Vol. 113, 2021, pp. 106708.

[26] Zhang, T., Qiao, G., Smith, D., Barakos, G., and Kusyumov, A., "Parametric study of aerodynamic performance of equivalent ducted/unducted rotors," *Aerospace Science and Technology*, Vol. 117, 2021, pp. 106984.

[27] Qiao, G., *Parametric study of aerodynamic performance of equivalent ducted/un-ducted propellers based on high-fidelity computational fluid dynamics*, Master's thesis, University of Glasgow, 2021, http://theses.gla.ac.uk/id/eprint/82702.

[28] Menter, F. R., "Two-equation eddy-viscosity turbulence models for engineering applications," *AIAA journal*, Vol. 32, No. 8, 1994, pp. 1598–1605.

[29] Qiao, G., Higgins, R. J., Barakos, G. N., and Zhang, T., "CFD Study of eVTOL Distributed Propulsors," *RAeS Applied Aerodynamics Conferencei, No.4 Hamilton Place, London, UK*, 13-15 September 2022.

[30] Biava, M. and Barakos, G. N., "Optimisation of ducted propellers for hybrid air vehicles using high-fidelity CFD," *The Aeronautical Journal*, Vol. 120, No. 1232, 2016, pp. 1632–1657.

[31] Chirico, G., Barakos, G. N., and Bown, N., "Propeller installation effects on turboprop aircraft acoustics," *Journal of Sound and Vibration*, Vol. 424, 2018, pp. 238–262.

[32] Chirico, G., Barakos, G. N., and Bown, N., "Numerical aeroacoustic analysis of propeller designs," *Aeronautical Journal*, Vol. 122, No. 1248, February 2018, pp. 283–315.

[33] Smith, D., Filippone, A., and Barakos, G., "Acoustic analysis of counter-rotating open rotors with a locked blade row," *AIAA Journal*, Vol. 58, No. 10, 2020, pp. 4401–4414.

[34] Qiao, G. and Barakos, G., "CFD Validation for eVTOL Propeller Performance and Acoustics," *49th European Rotorcraft Forum (ERF), paper 20, Bückeburg, Germany*, September 5 – 7, 2023.

[35] Yin, J., De Gregorio, F., Rossignol, K.-S., Rottmann, L., Ceglia, G., Reboul, G., Barakos, G., Qiao, G., Muth, M., Kessler, M., Visingardi, A., Barbarino, M., Petrosino, F., Zanotti, A., Oberti, N., Galimberti, L., Bernardini, G., Poggi, C., Abergo, L., Caccia, F., Guardone, A., Testa, C., and Zaghi, S., "Acoustic and Aerodynamic Evaluation of DLR Small-Scale Rotor Configurations within GARTEUR AG26," *49th European Rotorcraft Forum (ERF), paper 80, Bückeburg, Germany*, September 5 – 7, 2023.

[36] De Gregorio, F., Rossignol, K.-S., Ceglia, G., and Yin, J., "Multi-rotor Wake Interaction Characterization," *49th European Rotorcraft Forum (ERF), paper 105, Bückeburg, Germany*, September 5 – 7, 2023.

[37] Yin, J., Rossignol, K.-S., Rottmann, L., and Schwarz, T., "Numerical Investigations on Small-scale Rotor Configurations with Validation Using Acoustic Wind Tunnel Data," *48th European Rotorcraft Forum (ERF), 2022*, 2022, pp. 1–17.

[38] Yin, J., Rossignol, K.-S., Rottmann, L., and Schwarz, T., "Numerical studies on small rotor configurations with validation using acoustic wind tunnel data," *CEAS Aeronautical Journal*, 2023, pp. 1–32.

[39] Rossignol, K.-S., Yin, J., and Rottmann, L., "Investigation of Small-Scale Rotor Aeroacoustic in DLR's Acoustic Wind Tunnel Braunschweig," *28th AIAA/CEAS Aeroacoustics 2022 Conference*, 2022, p. 2838.